

*ten*SVD algorithm for compression

Michele Gallo

^a*University of Naples - L'Orientale, Department of Human and Social Sciences L.go
S.Giovanni Maggiore, 30 Naples, 80134, Italy mgallo@unior.it*

Abstract

Tensors provide a robust framework for managing high-dimensional data. Consequently, tensor analysis has emerged as an active research area in various domains, including machine learning, signal processing, computer vision, graph analysis, and data mining. This study introduces an efficient image storage approach utilizing tensors, aiming to minimize memory to store, bandwidth to transmit and energy to processing. The proposed method organizes original data into a higher-order tensor and applies the Tucker model for compression. Implemented in R, this method is compared to a baseline algorithm. The evaluation focuses on efficient of algorithm measured in term of computational time and the quality of information preserved, using both simulated and real datasets. A detailed analysis of the results is conducted, employing established quantitative metrics, with significant attention paid to sustainability in terms of energy consumption across algorithms.

Keywords:

Tucker decomposition, Tensor compression, Tucker3, HOSVD, Image and video processing, Sustainability

1. Introduction

A significant volume and complexity of image and video datasets are continuously generated by modern devices every second. These data necessitate continuous improvement of methods to reduce storage space and processing time, thereby facilitating more efficient extraction and transmission of information. It is well known that there are two major categories of methods to reduce memory space, with compression being one. The first category is based on a lossless compression strategy, while the second relies on lossy compression. The latter guarantees substantial reductions in memory cost

while maintaining a high percentage of the original information. Ongoing research endeavors persist in exploring and developing innovative methods to address the challenges associated with compression tasks.

To this end, a diverse array of methodologies has been proposed across various disciplines, including astronomy, biology, chemistry, engineering, geology, and medical imaging. Several comprehensive surveys have been conducted to organize the different approaches employed in these domains, notably [2] and [3], which are recent surveys comparing several techniques for image and video compression.

Image compression is effectively achieved using multivariate techniques such as Singular Value Decomposition (SVD) [4], [5]. While grayscale images are typically represented as two-dimensional matrices, color images are commonly structured in three dimensions (RGB channels). These multivariate methods can be applied to diminish the dimensionality of each color channel independently. However, such approaches become inefficient when dealing with videos or more complex signals that necessitate consideration of higher-dimensional data.

Consequently, methodologies such as Tucker analysis [6] and broader tensor decompositions are increasingly leveraged for compression purposes. For an overview of tensor decomposition models, refer to [7]. These approaches are better equipped to manage the complexity inherent in high-quality images or videos and their conversion into higher dimensional data, thereby enhancing both compression efficiency and overall performance.

A significant bottleneck for all compression methods is achieving the extraction of only the useful information contained in high-resolution images or videos. In this way, a low storage footprint is needed while maintaining an acceptable level of quality. The trade-off between reduced storage and the details and clarity of images or videos is consistently considered in compression contexts. Additionally, the time required for compression processes is a critical factor in signal transmission, as it directly influences transmission efficiency and bandwidth utilization. Rarely is compression studied as a fundamental tool for achieving a more sustainable processing of images and videos. However, concerns regarding the energy consumption of data centers are rapidly increasing, as much of the energy they consume is for processing and archiving the millions of images and videos collected daily. Thus, more attention needs to be paid when developing algorithms for image and video compression.

Based on tensor decomposition, a novel algorithm is proposed for this pur-

pose, called *tenSVD* (tensor Singular Value Decomposition). It is designed to ensure high sustainability in terms of energy consumption while balancing the trade-off between storage and quality requirements.

To determine effectiveness, the *tenSVD* is compared to the established algorithm for Tucker analysis, High Order Singular Value Decomposition (HOSVD) [8]. The strengths and weaknesses of *tenSVD* are analyzed using several metrics, including Peak Signal-to-Noise Ratio (PSNR), Mean Squared Error (MSE), and Processing Time (TIME).

The remainder of this article is structured as follows: Section 2 introduces tensors, including preliminary concepts. Section 3 presents the main idea of the proposed approach and the relative algorithm. A case study with full comparative results is provided in Section 4. Finally, conclusions and findings are presented in Section 5.

2. Tensor Decomposition

The Tucker model (Tucker3) is one of the most cited and widely applied methods for tensor decomposition. Originally proposed for three-way cases, it is referred to in several ways, including Three-Mode Principal Component Analysis (3MPCA), N-Mode Components Analysis (N-Mode PCA), and Higher-Order SVD (HOSVD) [6, 9, 10, 8]. Today, the Tucker model has been generalized to higher-order tensors and is rapidly increasing its application in imaging analysis [11]. For clarity, some preliminary concepts and notations will be recalled in Section 2.1, which will be used throughout the paper.

2.1. Preliminary Concepts and Notations

Objects with more than two indices are referred to as multi-way arrays, whereby the number of indices is termed the order. Nowadays, it is common to refer to any multi-way array as a tensor, and we maintain this tradition to identify the linear operators along with their multidimensional counterparts [12].

A real-valued tensor $\mathcal{X} \in \mathbb{R}$ of order $N \in \mathbb{N}$ is denoted by indices $(I_1 \times \cdots \times I_N)$, and its entries are denoted by $x_{i_1 \dots i_N}$. When only a fixed subset of indices is considered, this part of the tensor is termed a *subtensor*. The fibers are defined by fixing all indices except for one, e.g., $\mathbf{x}(:, i_2, i_3, \dots, i_N)$, and slices are obtained by fixing all but two indices, e.g., $\mathbf{X}(:, :, i_3, \dots, i_N)$.

Tensors can be reformatted in several ways, with one particular case of manipulation known as n -mode unfolding or matrix unfolding. Denoted by $\mathbf{X}(n)$, the n -mode unfolding of a tensor \mathcal{X} arranges the n -mode fibers as columns in the resulting matrix: $\mathbf{X}(n)$ ($I_n \times \prod_{i \neq n} I_i$).

According to Kolda and Bader [13], tensor products involved are significantly more complex compared to matrices.

Let $\mathcal{X}(I_1 \times \cdots \times I_n \times \cdots \times I_N)$ and $\mathbf{U}(H \times I_n)$ be defined as follows:

$$\mathcal{Y} = \mathcal{X} \times_n \mathbf{U}$$

where $\mathcal{Y}(I_1 \times \cdots \times H \times \cdots \times I_N)$, and \times_n is the n -mode product of a tensor. The norm of a tensor \mathcal{X} is analogous to the Frobenius norm and is defined as the square root of the sum of the squares of all its elements:

$$\|\mathcal{X}\| = \sqrt{\sum_{i_1=1}^{I_1} \sum_{i_2=1}^{I_2} \cdots \sum_{i_N=1}^{I_N} x_{i_1 i_2 \dots i_N}^2}$$

The inner product of two same-sized tensors \mathcal{X} and \mathcal{Y} is the sum of the products of their corresponding entries:

$$\langle \mathcal{X}, \mathcal{Y} \rangle = \sum_{i_1=1}^{I_1} \sum_{i_2=1}^{I_2} \cdots \sum_{i_N=1}^{I_N} x_{i_1 i_2 \dots i_N} y_{i_1 i_2 \dots i_N}$$

The rank of a tensor is thoroughly different from its matrix counterpart. Specifically, \mathcal{X} has a rank- (R_1, R_2, \dots, R_N) , known as multilinear rank, where R_n is the dimension of vector space spanned by the n -mode vectors:

$$R_n = \text{rank}_n(\mathcal{X}) = \text{rank}(\mathbf{X}_{(n)})$$

with $R_n \leq I_n$ for all $n = 1 \dots N$.

2.2. TUCKER MODEL

In accordance with the notation given in Section 2.1, the Tucker model for an N th order tensor can be expressed as

$$\mathcal{X} \approx \mathcal{G} \times_1 \mathbf{U}^{(1)} \times_2 \mathbf{U}^{(2)} \cdots \times_n \mathbf{U}^{(n)} \cdots \times_N \mathbf{U}^{(N)} \quad (1)$$

where $(n = 1, 2, \dots, N)$ and each $\mathbf{U}^{(n)}(I_n \times R_n)$ is an orthonormal component matrix ($\mathbf{U}^{(n)t} \mathbf{U}^{(n)} = \mathbf{I}$); \mathcal{G} is the core tensor with dimension $(R_1 \times R_2 \times \cdots \times$

R_N).

Assuming $N = 2$ with dimension $(I_1 \times I_2)$, and R_1 and R_2 representing the dimensions of the vector space spanned by the first and second modes, respectively, the Tucker decomposition can be written as

$$\mathcal{X} \approx \mathcal{G} \times_1 \mathbf{U}^{(1)} \times_2 \mathbf{U}^{(2)} \quad (2)$$

where $\mathbf{U}^{(1)}(I_1 \times R_1)$ and $\mathbf{U}^{(2)}(I_2 \times R_2)$ are orthonormal component matrices, and \mathcal{G} is the core tensor with dimension $(R_1 \times R_2)$.

It can be demonstrated that $\mathbf{U}^{(1)}$ and $\mathbf{U}^{(2)}$ are the left and right singular vectors of \mathcal{X} , while the core tensor is a matrix that contains singular values on the first r diagonal elements ($r = \min(R_1, R_2)$) and zeros otherwise.

It is important to underline that the core tensor for $N > 2$ is a full tensor, where its elements can also be negative. The magnitude of these elements indicates the strength of the interaction between components represented by the corresponding indices in the component matrices.

2.3. Tucker Parameters Estimation

The Tucker decomposition of a 2nd order tensor is equivalent to a Singular Value Decomposition (SVD). Thus, it is not surprising that Higher-Order Singular Value Decomposition (HOSVD) is the most popular algorithm for estimating the parameters of a Tucker model in cases where $N > 2$.

Introduced by De Lathauwer et al. [8], which generalizes the three-way case presented by Tucker [6], HOSVD finds the exact Tucker decomposition of rank- (R_1, R_2, \dots, R_N) and subsequently provides the core tensor \mathcal{G} . In essence, HOSVD initially computes the left singular vectors of $\mathbf{X}_{(n)}$ for $n = 1, 2, \dots, N$. Finally, the transposes of these matrices are multiplied with the original tensor \mathcal{X} to obtain the core tensor.

When exact parameters are not required, such as in the case of lossy compression, only the first r_n columns of $\mathbf{U}^{(n)}$ are considered. The objective function to solve is defined as follows:

$$\|\mathcal{X} - \mathcal{G} \times_1 \mathbf{U}^{(1)} \times_2 \mathbf{U}^{(2)} \dots \times_n \mathbf{U}^{(n)} \dots \times_N \mathbf{U}^{(N)}\|^2 \quad (3)$$

where $\mathbf{U}^{(n)}(I_n \times r_n)$ is orthonormal, and \mathcal{G} has dimensions $(r_1 \times r_2 \times \dots \times r_N)$. The details of the optimization problem are readily available in [8, 13]. The version of HOSVD used to estimate the parameters is referred to as *truncated* HOSVD (*t*-HOSVD), which is briefly described below, highlighting its

simplicity and limited number of steps.

Algorithm 1: t -HOSVD

Require: Tensor \mathcal{X} (I_1, I_2, \dots, I_N) and (r_1, r_2, \dots, r_N)

for n in $1, \dots, N$ **do**

 Consider the unfolding $\mathbf{X}_{(n)}$

 Compute the $\text{SVD}(\mathbf{X}_{(n)})$

$\mathbf{U}^{(n)} \leftarrow r_n$ left singular vectors of $\mathbf{X}_{(n)}$

end for

$\mathcal{G} \leftarrow \mathcal{X} \times_1 \mathbf{U}^{(1)t} \times_2 \mathbf{U}^{(2)t} \times_3 \dots \times_N \mathbf{U}^{(N)t}$

return $\mathcal{G}, \mathbf{U}^{(1)} \dots \mathbf{U}^{(n)} \dots \mathbf{U}^{(N)}$

end

Based on a lossless compression strategy, HOSVD can significantly reduce the memory cost of the original tensor. Its effectiveness is determined by rank – (R_1, R_2, \dots, R_N) compared to the dimensions of the modes (I_1, I_2, \dots, I_N) . In fact, the original memory cost of \mathcal{X} is $\prod_{n=1}^N I_n$, while the memory cost of HOSVD is given by the sum of smaller matrices plus a core tensor, specifically $\sum_{n=1}^N I_n \times R_n$ for the component matrices and $\prod_{n=1}^N R_n$ elements for core tensor.

Differently, by choosing $r_1 \ll R_1, r_n \ll R_n, \dots, r_N \ll R_N$, t -HOSVD assures a higher compression while still capturing the essential structure of the original tensor. However, the choice of parameters (r_1, r_2, \dots, r_N) directly influences the balance between compression (memory savings) and accuracy (quality of the reconstruction of the original tensor).

Another crucial aspect to consider when algorithms are used for compression is their computational efficiency in terms of FLOPs (floating point operations per second). In the HOSVD algorithm, SVD is used to decompose N flattened matrices $\mathbf{X}_{(n)}$, with $I_n \ll I$ ($I = \prod_{i \neq n} I_i$). Thus, the computational cost for these steps is given by the sum of N individual SVDs:

$$\sum_{n=1}^N (I_n I^2 + \mathcal{O}(I^3)). \quad (4)$$

3. tenSVD for Compression

In the context of data compression, assuming fixed accuracy for images or videos, the goal is to maximize compression or save memory space. Similarly,

we introduce the *tenSVD* algorithm; however, we first want to focus on computational cost and its impact on energy consumption and processing time.

3.1. Computational Cost

From Section 2.3, it is easy to verify that the left singular vector of each $\mathbf{X}_{(n)}$ has $\mathcal{O}(I_n I^2 + I^3)$ FLOPs. On the other hand, it is clear that calculating the left singular vectors of $\mathbf{X}_{(n)} \mathbf{X}_{(n)}^t$ requires less computational overhead. In fact, we need $\mathcal{O}(I I_n^2)$ FLOPs for multiple $\mathbf{X}_{(n)}$ with its transpose, and $\mathcal{O}(I_n^3)$ for the SVD of $\mathbf{X}_{(n)} \mathbf{X}_{(n)}^t$. Thus, the total cost to obtain the left singular vectors is $\mathcal{O}(I I_n^2 + I_n^3)$.

Following this approach, the FLOPs required by HOSVD are given by

$$\sum_{n=1}^N \mathcal{O}(I_n I^2 + I_n^3). \quad (5)$$

Since $I_n \ll I$, $\mathcal{O}(I^3)$ is greater than $\mathcal{O}(I_n^3)$.

Based on this consideration, the primary concept of the new approach involves rearranging all elements of an N th-order tensor \mathcal{X} into an M th-order tensor \mathcal{Z} with $(M \ll N)$. Let (I_1, I_2, \dots, I_N) and (J_1, J_2, \dots, J_M) represent the dimensionality of \mathcal{X} and \mathcal{Z} , respectively. In this transformation, we have $I_n \geq J_m$ for all m and n , ensuring that the total number of elements remains conserved through rearrangement, such that:

$$\prod_{n=1}^N I_n = \prod_{m=1}^M J_m.$$

Let $J = \prod_{j \neq m} J_j$. The computational cost of M matrices $\mathbf{Z}_{(m)} \mathbf{Z}_{(m)}^t$ is given by

$$\sum_{m=1}^M \mathcal{O}(J_m J^2 + J_m^3). \quad (6)$$

It is easy to observe that $J_m J^2$ and $I_n I^2$ are the dominant terms in equations 6 and 5, which outweigh the cubic terms J_m^3 and I_n^3 , respectively. Hence, the reordering of the elements across more modes reduces the computational cost from $\sum_{n=1}^N I_n I^2$ to $\sum_{m=1}^M J_m J^2$.

3.2. Memory Cost

When lossy compression is the strategy, to reduce memory cost, the parameters (r_1, r_2, \dots, r_N) are fixed lower than (R_1, R_2, \dots, R_N) . In the case where the elements are reordered into a higher-order tensor, it is not clear whether the memory cost will be higher. The storage requirements are given by the sum of the memory costs for each component matrix, represented as $\sum_{n=1}^N I_n \times r_n$, and the core tensor, represented as $\prod_{n=1}^N r_n$. If the elements are rearranged into an M th-order tensor, the memory storage required will be $\sum_{m=1}^M (J_m \times r_m) + \prod_{m=1}^M r_m$. Thus, it is clear that the dominant memory cost arises from the core tensor.

On the other hand, it can be shown that the sum of the squares of the elements of a tensor is equal to the sum of the squares of the elements of the core tensor, expressed as follows:

$$\begin{aligned}
& \left\| \mathcal{Z} - \mathcal{G} \times_1 \mathbf{U}^{(1)} \times_2 \mathbf{U}^{(2)} \dots \times_m \mathbf{U}^{(m)} \dots \times_M \mathbf{U}^{(M)} \right\|^2 \\
&= \|\mathcal{Z}\|^2 - 2 \langle \mathcal{Z} \times_1 \mathbf{U}^{(1)t} \times_2 \mathbf{U}^{(2)t} \dots \times_m \mathbf{U}^{(m)t} \dots \times_M \mathbf{U}^{(M)t}, \mathcal{G} \rangle + \|\mathcal{G}\|^2 \\
&= \|\mathcal{Z}\|^2 - 2 \langle \mathcal{G}, \mathcal{G} \rangle^2 + \|\mathcal{G}\|^2 \\
&= \|\mathcal{Z}\|^2 - \|\mathcal{G}\|^2.
\end{aligned}$$

It is also demonstrated that the sum of the squares of the core tensor is concentrated in a relatively small number of elements. Based on these two considerations, it may be reasonable to consider and save only the elements of the core that have the highest squared values. Moreover, instead of saving a fixed number of columns for each component matrix, i.e., $\mathbf{U}(J_m \times r_m)$ for $m = 1, \dots, M$, and a core tensor with corresponding dimensions, it is possible to save the full component matrices, i.e., $\mathbf{U}(J_m \times J_m)$ for $m = 1, \dots, M$, and only the elements of the core tensor with the highest magnitudes, ensuring that the ratio of the collected sum of squares to the total sum of squares is as high as desired.

3.3. *tenSVD* Algorithm

To show the main phases of the *tenSVD* procedure, in Figure 1 a matrix (2nd order tensor) is reshaped into a 3rd order ones.

According to several strategies, such as compression ratio or the percentage of original information to retain, the quality measure of the original object

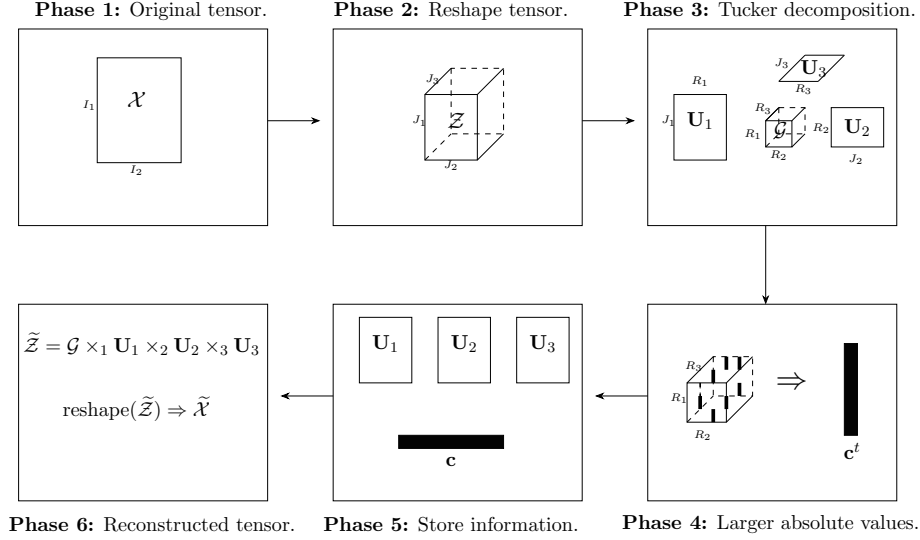


Figure 1: *tenSVD* framework.

is determined in Phase 1. In Phase 2, the order and dimensions of the new object must be established, where the order is higher than that of the original tensor, and the dimensions for each mode are lower. Heuristically, we have observed that *tenSVD* is more efficient when the new tensor approaches the shape of a hypercube.

In Phase 3, component matrices and the core tensor are calculated using SVD. Elements of the core tensor with the highest magnitudes are selected to ensure the desired level of quality in Phase 4. In Phase 5, the component matrices and selected elements, along with their relative positions in the core tensor, are saved in $\mathbf{U}^{(m)}$ ($m = 1 \dots M$) and \mathbf{c} , respectively. The data saved in this phase could be stored or transmitted to conserve space (in the case of backup) and bandwidth (in the case of transmission). In the final phase, the saved information is used to reconstruct the approximated original image.

The steps of *tenSVD* are detailed in Algorithm 2, where it is possible to observe that both accuracy (given by Relative Error ϵ) and compression (given by compression ratio *com*) can be fixed.

Algorithm 2: *tenSVD*

Require: Tensor $\mathcal{X}(I_1, I_2, \dots, I_N)$; ϵ (or com)
Reshape $\mathcal{X} \Rightarrow \mathcal{Z}(J_1, J_2, \dots, J_J)$,
with $J_1 \cong J_2 \cong \dots \cong J_M \cong M$ and $\prod_{i=1}^N I_i = \prod_{m=1}^M J_m$
for m in $1, \dots, M$ **do**
 Consider the unfolding $\mathbf{Z}_{(m)}$ of \mathcal{Z}
 $\mathbf{U}^{(m)} \leftarrow R_m$ left singular vectors of $\text{SVD}(\mathbf{Z}_{(m)} \mathbf{Z}_{(m)}^t)$
end for
 $\text{dim} \leftarrow \text{size}(\mathbf{U}^{(1)}) + \dots + \text{size}(\mathbf{U}^{(M)})$
 $\mathcal{G} \leftarrow \mathcal{Z} \times_1 \mathbf{U}^{(1)t} \times_2 \mathbf{U}^{(2)t} \times_3 \dots \times_M \mathbf{U}^{(M)t}$
Select element of \mathcal{G}
 $\mathbf{g} \leftarrow \text{vec}(\text{abs}(\mathcal{G}))$
Order in decreasing way the elements of \mathbf{g}
 $r \leftarrow 1$
 $\hat{\mathbf{g}} \leftarrow 0$
while $\|\text{sum}(\mathbf{g}) - \text{sum}(\hat{\mathbf{g}})\| / \|\text{sum}(\mathbf{g})\| \geq \epsilon$ (or $\text{dim}/\text{size}(\mathcal{Z}) \leq \text{com}$) **do**
 $\hat{\mathbf{g}} \leftarrow \hat{\mathbf{g}} + \mathbf{g}[r]$
 $r \leftarrow r + 1$
 Set in \mathbf{c} the elements of \mathcal{G} selected and their relative position
 $\text{dim} \leftarrow \text{dim} + \text{size}(\mathbf{c})$
end while
return $\mathbf{c}, \mathbf{U}^{(1)} \dots \mathbf{U}^{(M)}, I_1 \dots I_N$
end

In the first stage of the procedure, the elements are rearranged into an M -order tensor with dimensions J_1, J_2, \dots, J_M . The total number of elements, i.e., $\prod_{i=1}^N I_i$, is divided into prime factors. The smaller values are aggregated in increasing order until the minimum of them is approximately equal to M . In the second stage, the HOSVD algorithm is applied to the new tensor \mathcal{Z} . The full left singular vectors and core tensor are calculated. From a computational point of view, it is more efficient to work on $\mathbf{Z}_{(m)} \mathbf{Z}_{(m)}^t$ than on the m -mode unfolding $\mathbf{Z}_{(m)}$.

In the final stage, the highest absolute values and their positions in the core tensor are selected as a vector, while ensuring that the fixed relative error or level of compression is achieved. Finally, these elements and component matrices are saved.

4. Case Study

The *tenSVD* algorithm was implemented in R to evaluate its performance for lossy compression. The algorithm was compared with the HOSVD algorithm (using the ‘*tenSR*’ package). The analysis was conducted on an Intel(R) Xeon(R) Gold 6288 CPU running at 2.10 GHz (16 cores) with 512 GB of RAM, and using R version 4.2.0.

Three images — the Veiled Christ, the Doryphoros of Polykleitos, and the Royal Palace of Caserta — are shown in Fig.2. These images were converted into datasets: Fig.2 (a) has 880 rows and 1,240 columns, Fig.2 (b) has 1,792 rows and 2,560 columns, and Fig.2 (c) has 7,200 rows and 5,400 columns, all represented with three channels (RGB). Thus, three third-order tensors with dimensions $(880 \times 1,240 \times 3)$, $(1792 \times 2560 \times 3)$, and $(7200 \times 5400 \times 3)$ were generated.

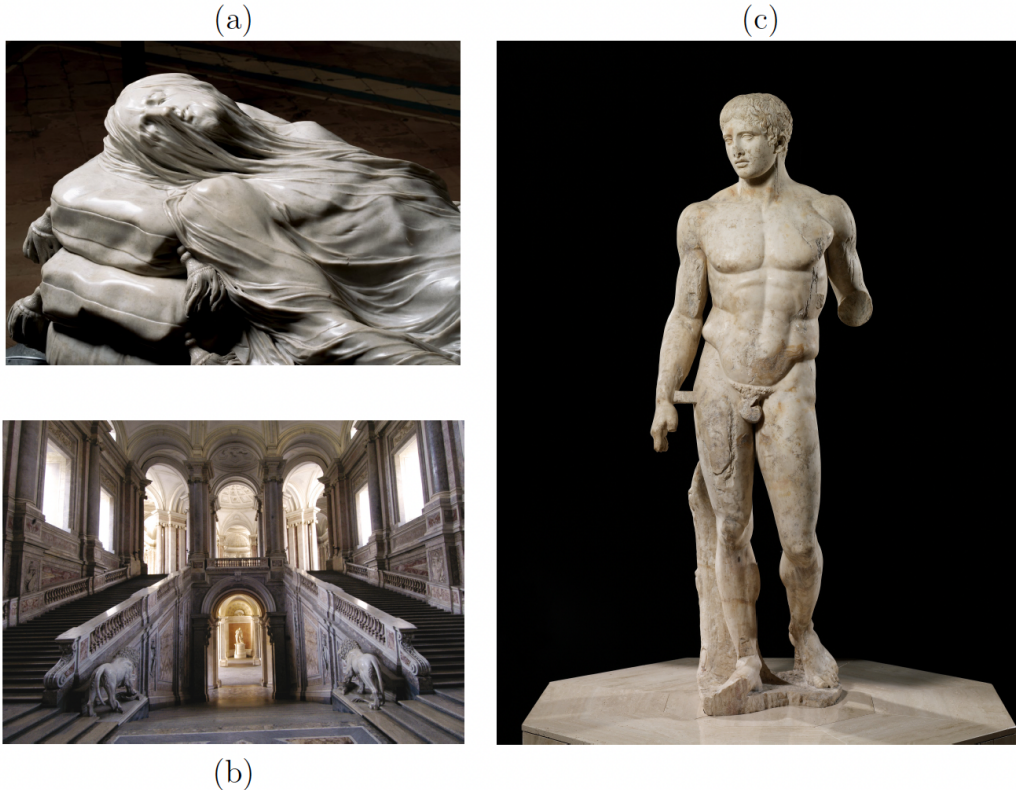


Figure 2: Veiled Christ (a), Royal Palace of Caserta (b), Dorophos (c)

Additionally, a short video of the Athletics 100 meters final at the Paris 2024 Olympic Games was acquired. The grDevices package (version 4.4.0) was used to convert the three images into tensors. The Av package (version 0.9) was used to split the video into PNG images at a rate of three images per second. These frames were then converted into a fourth tensor with dimensions $(30 \times 360 \times 640 \times 3)$.

4.1. Evaluation Metrics

Mean Squared Error (MSE), Relative Error (ERR) and Peak-Signal-to-Noise Ratio (PSNR) are widely used to measure the accuracy of Tucker decomposition, while PSNR specifically assesses the quality of compressed images or videos.

- MSE is the square of the Frobenius norm of the difference between predicted and observed values of a tensor, normalized by the number of tensor elements:

$$\text{MSE} = \frac{\|\mathcal{X} - \hat{\mathcal{X}}\|^2}{I_1 * I_2 * \dots * I_N}$$

- ERR quantifies the difference between the original tensor and its approximation, normalized by the magnitude of the original tensor

$$\text{ERR} = \frac{\|\mathcal{X} - \hat{\mathcal{X}}\|}{\|\mathcal{X}\|}$$

- PSNR computes the peak signal-to-noise ratio between two images in decibels (dB). This ratio is a quality measurement between original and compressed image. PSNR can take values up to infinity; the higher the PSNR, the better the compressed image quality:

$$\text{PSNR} = 10 \log_{10} \left(\frac{\max(\max(\mathcal{X}), \max(\hat{\mathcal{X}}))^2}{\sqrt{\text{MSE}}} \right)$$

Moreover, to measure compression effectiveness in term of space and time, two additional metrics are used:

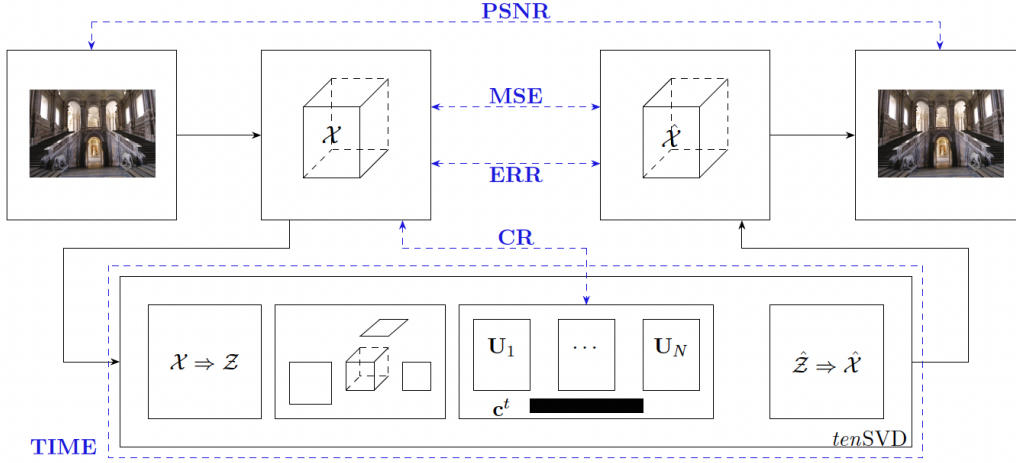


Figure 3: Used measurement protocol

- Compression Ratio (CR) is defined as the ratio between the size of the original tensor and the number of elements in the compression representation (storage cost).

$$\text{CR} = \frac{\text{compressed data size}}{\text{original data size}}$$

- Processing time (TIME) refers to the actual elapsed time from the start of the algorithm execution.

The detailed scheme of the developed framework is shown in Figure 3.

4.2. Results

To compress the images, three different sets of parameters were chosen for HOSVD: $r_1 = 100, r_2 = 100, r_3 = 3$ (a); $r_1 = 200, r_2 = 200, r_3 = 3$ (b); and $r_1 = 600, r_2 = 600, r_3 = 3$ (c). The CR values observed from HOSVD were used as parameters for *tenSVD* to obtain comparable results in terms of memory cost.

In Figures 4, 5, and 6, the reconstructed images are displayed, with HOSVD results shown on the upper side and *tenSVD* results on the bottom side. The different scenarios demonstrate that both algorithms provide the same accuracy in terms of quality.

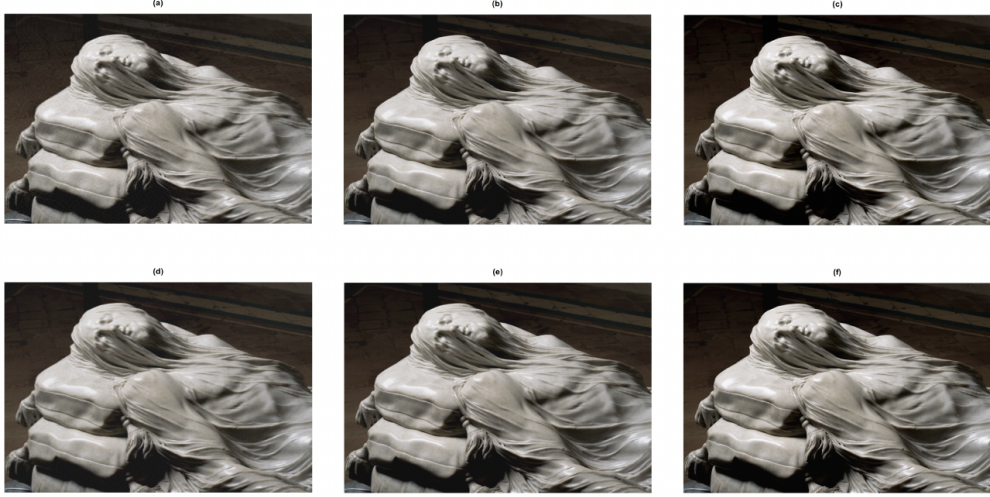


Figure 4: HOSVD CR= 93.7% (a), CR= 83.4% (b), and CR= 28.2% (c); *tenSVD* CR= 93.7% (d), CR= 83.4% (e), and CR= 28.2% (f).



Figure 5: HOSVD CR= 96.6% (a), CR= 92.8% (b), and CR= 83.2% (c); *tenSVD* CR= 96.6% (d), CR= 92.8% (e), and CR= 83.2% (f).

In Table 1, all diagnostic measures are summarized. It is clear that all scenarios show very comparable values in terms of accuracy and quality, as

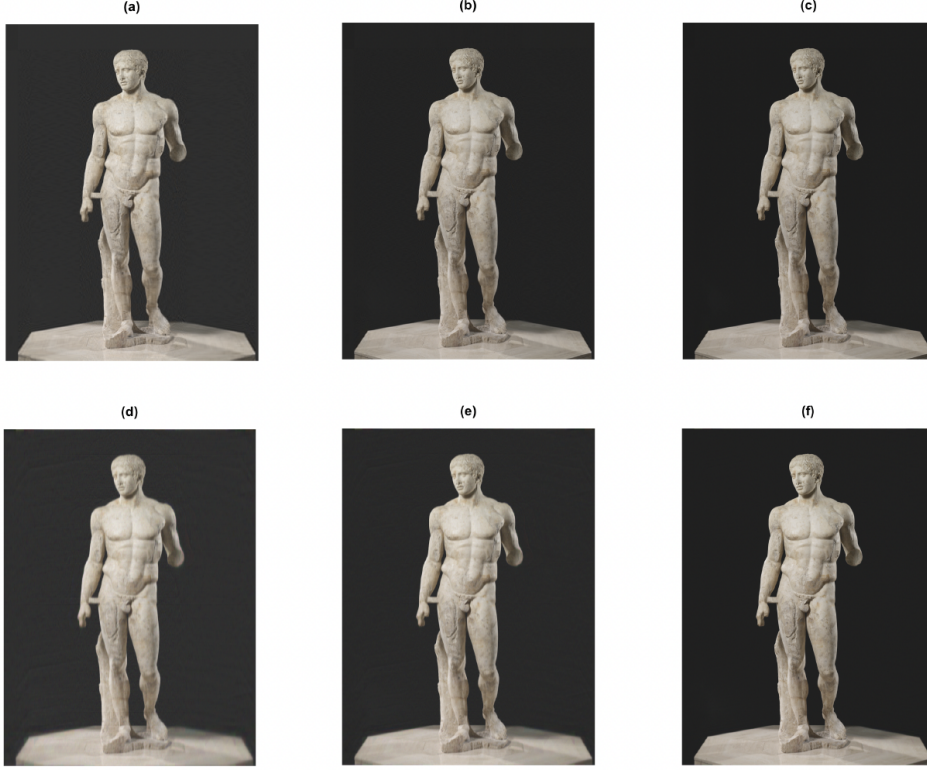


Figure 6: HOSVD CR= 98.9% (a), CR= 97.7% (b), and CR= 92.5% (c); *tenSVD* CR= 98.9% (d), CR= 97.7% (e), and CR= 92.5% (f).

demonstrated in Figures 4, 5, and 6. However, with fixed compression ratios, it is evident that *tenSVD* consistently provides better efficiency. Specifically, it is four times faster than HOSVD for the Veiled Christ and 26 times faster for the Doryphoros of Polykleitos, with both results based on scenario (c).

Regarding the Olympic Games Paris 2024 videos, a fixed set of parameters was analyzed: $r_1 = 30$, $r_2 = 300$, $r_3 = 300$, $r_4 = 3$. The HOSVD yielded the following metrics: MSE= 0.0013, ERR= 0.0594, PSNR= 28, CR= 41%. In contrast, *tenSVD* analyzed the same compression ratio, producing comparable metrics: MSE= 0.0036, ERR= 0.0952, PSNR= 24. The *tenSVD* algorithm was approximately 2.5 times faster than HOSVD (22.024 seconds vs. 54.403 seconds). In Figure 7 presents the original frames 1, 10, 15, 20, and 30 (on the left side), the reconstructed frames after HOSVD (in the center), and the reconstructed frames after applying *tenSVD* (on the

Image		Alg.	Metrics				
			CR	Time	PSNR	MSE	ERR
Figure 4	(a)	H	93.7%	28	24.2	0.0037	0.147
		T	93.7%	5	23.8	0.0041	0.157
	(b)	H	83.4%	29	27.5	0.0017	0.103
		T	83.4%	5	27.0	0.0019	0.108
	(c)	H	28.2%	33	38.9	0.0001	0.027
		T	28.2%	8	34.9	0.0003	0.043
Figure 5	(a)	H	96.6%	271	25.3	0.0029	0.107
		T	96.6%	24	24.5	0.0034	0.118
	(b)	H	92.8%	273	26.2	0.0023	0.099
		T	92.8%	27	26.0	0.0024	0.101
	(c)	H	83.2%	286	28.2	0.0015	0.101
		T	83.2%	31	29.5	0.0011	0.087
Figure 6	(a)	H	98.9%	6681	16.0	0.0252	0.94
		T	98.9%	248	15.5	0.0281	0.99
	(b)	H	97.7%	6703	18.4	0.0143	0.685
		T	97.7%	240	18.6	0.021	0.855
	(c)	H	92.5%	6859	20.0	0.0099	0.57
		T	92.5%	257	19.1	0.0128	0.64

Table 1: Performance comparison of HOSVD (H) and *ten*SVD (T) for the Veilled Christ, the Royal Palace of Caserta and the Doryphoros of Polykleitos with different compression ratio scenarios.

right side).

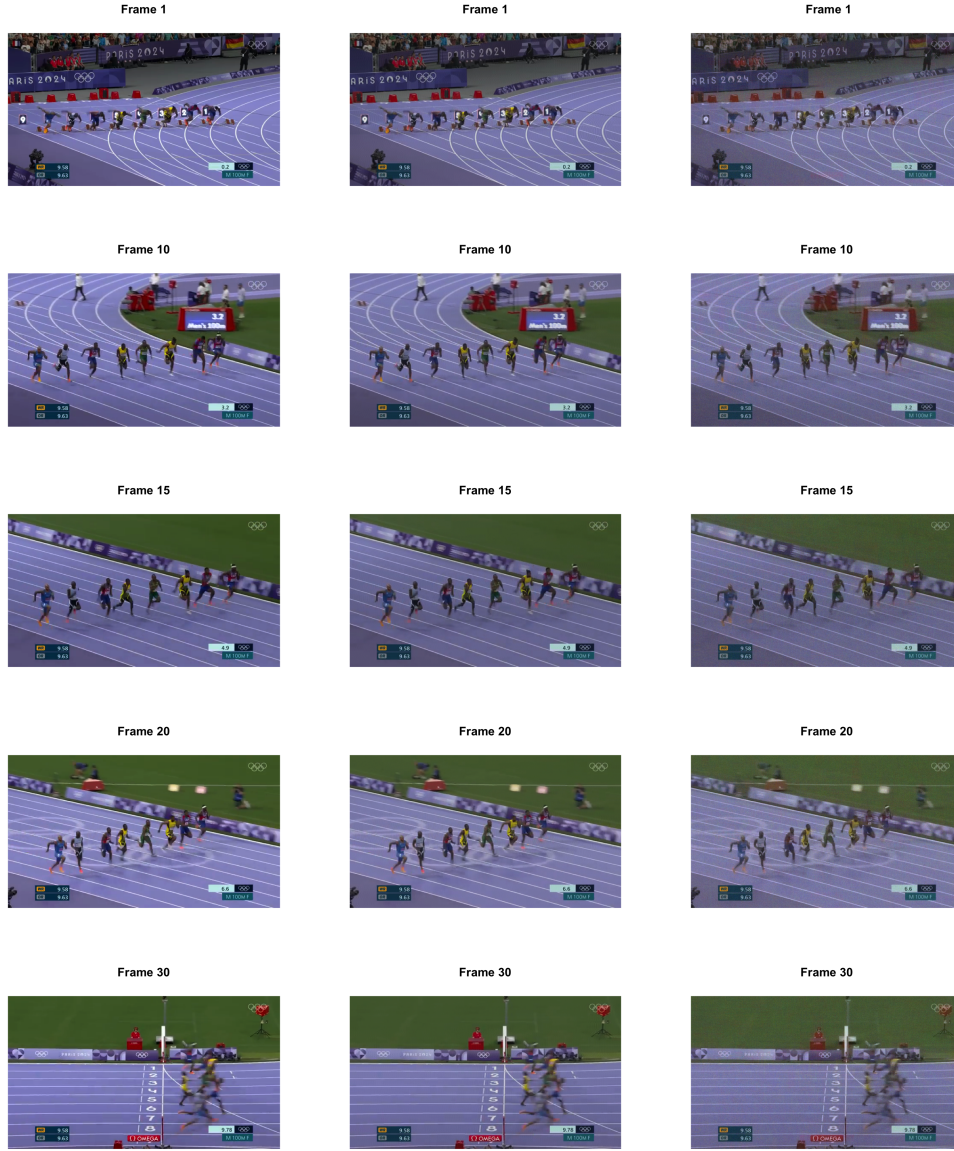


Figure 7: Frames 1, 10, 15, 20, 30, original on left side, HOSVD on central and *tenSVD* on right side

5. Conclusion and Findings

For the same level of quality and compression, it has been demonstrated that *tenSVD* is a faster algorithm compared to HOSVD. Moreover, the re-

sults indicate that the speed improvement can be quite significant in several scenarios. In Table 1, it can be observed that, on average, *tenSVD* is about 5.8 times faster than HOSVD for the 3,273,600 elements of the $880 \times 1,240 \times 3$ tensor, 10.1 times faster for the 13,762,560 elements of the $1,792 \times 2,560 \times 3$ tensor, and 27.9 times faster for the 32,531,040 elements of the $2,378 \times 4,560 \times 3$ tensor. In the case of the $30 \times 360 \times 640 \times 3$ tensor, it is 2.5 times faster. Thus, the difference in computational time depends more on the shape of the tensor than on its size.

To further verify this, a simulation study was conducted on eight different image standards: $1280 \times 720 \times 3$ (HD), $1920 \times 1080 \times 3$ (Full HD), $2048 \times 1080 \times 3$ (2K), $2560 \times 1440 \times 3$ (4K), $3840 \times 2160 \times 3$ (4K UHD), $5120 \times 2880 \times 3$ (5K), $6144 \times 3456 \times 3$ (6K), and $7680 \times 4320 \times 3$ (8K). Datasets were generated 25 times using a uniform distribution. The times were measured in seconds, and summary statistics are given in Appendix A.

Figure 8 illustrates the elapsed time ratio between the two algorithms, showing that *tenSVD* is consistently faster than HOSVD, with the best results noted for the EK scenario.

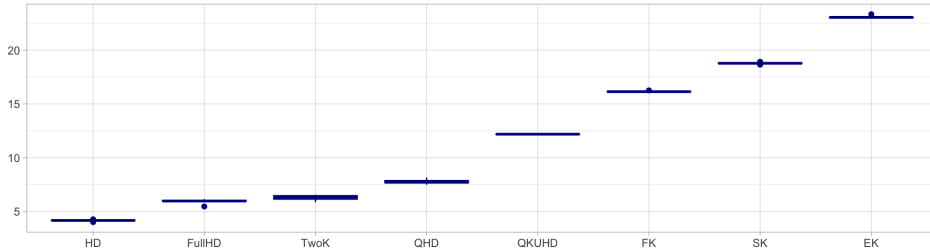


Figure 8: Elapsed time ratio between HOSVD and *tenSVD* for scenario $1280 \times 720 \times 3$ (HD), $1920 \times 1080 \times 3$ (FullHD), $2048 \times 1080 \times 3$ (TwoK), $2560 \times 1440 \times 3$ (4HD), $3840 \times 2160 \times 3$ (QKUHD), $5120 \times 2880 \times 3$ (FK), $6144 \times 3456 \times 3$ (SK), and $7680 \times 4320 \times 3$ (EK)

It appears that *tenSVD* is more efficient when it can reshape the original tensor into a form close to a hypercube. Other factors that influence efficiency include the initial shape of the tensor. In the case of higher quality images, the tensor is necessarily highly unbalanced because one mode has a dimension of 3 (RGB channels). In such cases, *tenSVD* demonstrates significant performance advantages in terms of computational cost.

Unfortunately, *tenSVD* is not suitable for several other applications. In situations where data is generated by latent variables, it cannot effectively

analyze the underlying latent variables that caused the data generation, as the original structure is lost when the tensor is reshaped into a higher-order form. If the total core energy does not change when the tensor is reshaped, it is not possible to obtain the true orthonormal component matrices. In this context, HOSVD remains effective, but its accuracy may be compromised in the presence of significant noise.

Iterative algorithms such as Higher Order Orthogonal Iteration (HOOI) [9, 8], Sequentially Truncated Higher-Order Singular Value Decomposition (*st*HOSVD) [14], and Gradient Descent methods generally yield higher accuracy [1]. These algorithms have the advantage of converging to a better fit and are generally versatile, allowing for adaptation to many different scenarios and constraints. However, their iterative nature may lead to convergence issues, possibly getting stuck in local minima, and they could be very expensive in terms of both time and energy consumption.

ACKNOWLEDGMENTS

Data availability statement The data used in the paper are available either through the provided link with supplementary material or R packages.

Funding This research did not receive any specific grant from funding agencies in the public, commercial, or not-for-profit sectors.

Declarations

Conflict of interest The authors have no conflict of interest.

Ethical Approval Simulated data was used in the assessment of the proposed methods.

Open Access This article is licensed under a Creative Commons Attribution 4.0 International License, which permits use, sharing, adaptation, distribution and reproduction in any medium or format, as long as you give appropriate credit to the original author(s) and the source, provide a link to the Creative Commons licence, and indicate if changes were made. The images or other third party material in this article are included in the article's Creative Commons licence, unless indicated otherwise in a credit

line to the material. If material is not included in the article’s Creative Commons licence and your intended use is not permitted by statutory regulation or exceeds the permitted use, you will need to obtain permission directly from the copyright holder. To view a copy of this licence, visit <http://creativecommons.org/licenses/by/4.0/>.

References

- [1] Yang P, Huang Y, Qiu Y, Sun W, Zhou G. 2022. A high-order tensor completion algorithm based on fully-connected tensor network weighted optimization. *Cham: Springer International Publishing*
- [2] Jamil S, Piran MJ, Rahman M, Kwon OJ. 2023. Learning-driven lossy image compression: A comprehensive survey. *Engineering Applications of Artificial Intelligence* 123:106361
- [3] Capitán-Vallvey LF, Lopez-Ruiz N, Martinez-Olmos A, Erenas MM, Palma AJ 2015. Recent developments in computer vision-based analytical chemistry: A tutorial review. *Analytica Chimica Acta* 899:23–56
- [4] Stewart GW. 1993. On the early history of the singular value decomposition. *SIAM review*, 35(4):551–566
- [5] Nayar SK, Nene SA, Murase H. 1996. Subspace methods for robot vision. *IEEE Transactions on Robotics and Automation*, 12(5):750–758
- [6] Tucker LR. 1966. Some mathematical notes on three-mode factor analysis. *Psychometrika*, 31(3):279–311
- [7] Nie C, Wang H, Zhao L. 2023. Adaptive tensor networks decomposition for high-order tensor recovery and compression. *Information Sciences*, 629:667–684
- [8] De Lathauwer L, De Moor B, Vandewalle J. 2000. On the best rank-1 and rank-(r_1, r_2, \dots, r_n) approximation of higher-order tensors. *SIAM journal on Matrix Analysis and Applications*, 21(4):1324–1342
- [9] Kroonenberg PM, De Leeuw J. 1980. Principal component analysis of three-mode data by means of alternating least squares algorithms. *Psychometrika*, 45:69–97

- [10] Kapteyn A, Neudecker H, Wansbeek T. 1986. An approach to n-mode components analysis. *Psychometrika*, 51:269–275
- [11] Bi X, Tang X, Yuan Y, Zhang Y, Qu A. 2021. Tensors in statistics. *Annual review of statistics and its application*, 8(1):345–368
- [12] Trendafilov N, Gallo M. 2021. Multivariate data analysis on matrix manifolds. *Springer International Publishing*
- [13] Kolda TG, Bader BW. 2009. Tensor decompositions and applications. *SIAM review*, 51(3):455–500
- [14] Fang Z, Yang X, Han L, Liu X. 2018. A sequentially truncated higher order singular value decomposition-based algorithm for tensor completion. *IEEE transactions on cybernetics*, 49(5):1956–1967

6. Appendix A

	min	lq	mean	median	uq	max
HD (t)	7.75	7.97	8.04	8.03	8.10	8.45
HD (h)	33.21	33.51	33.59	33.55	33.72	34.02
FullHD (t)	19.49	19.94	20.29	20.09	20.32	22.22
FullHD (h)	119.94	120.69	120.84	120.80	121.12	121.62
TwoK (t)	20.89	21.35	21.97	21.72	22.59	23.69
TwoK (h)	137.18	137.68	138.18	137.95	138.78	139.05
QHD (t)	35.31	36.68	37.37	37.58	38.03	38.92
QHD (h)	288.67	289.53	290.03	289.99	290.47	292.42
QKUHD (t)	82.17	82.74	83.03	83.04	83.30	83.96
QKUHD (h)	1003.99	1009.48	1012.02	1011.04	1013.03	1024.94
FK (t)	149.11	150.62	151.08	151.12	151.48	153.14
FK (h)	2423.87	2432.26	2439.48	2436.27	2445.77	2465.66
SK (t)	220.18	222.90	223.71	223.36	225.21	227.10
SK (h)	4170.06	4196.02	4204.57	4202.03	4213.83	4238.27
EK (t)	348.56	354.64	355.35	355.99	356.93	358.65
EK (h)	8129.40	8154.86	8186.39	8178.94	8208.11	8262.79

Table 2: Algorithm comparison in terms of computation time for *ten*SVD (t) and HOSVD (h) on standard images. For each simulation scenario are used 25 different datasets generated from a uniform distribution. Results are reported as minimum (min), lower quartile (lq), mean, median, upper quartile (uq), and maximum (max).